JOURNAL OF PROPULSION AND POWER
Vol. 24, No. 6, November–December 2008

Exact Navier–Stokes Solution for Pulsatory Viscous Channel Flow with Arbitrary Pressure Gradient

J. Majdalani
University of Tennessee Space Institute, Tullahoma, Tennessee 37388

DOI: 10.2514/1.37815

In this article, an exact solution of the Navier–Stokes equations is presented for the motion of an incompressible viscous fluid in a channel with arbitrary pressure distribution. A generalization is pursued by expressing the pressure signal in terms of Fourier coefficients. The flow is characterized by two principal parameters: the pulsation parameter based on the periodic pressure gradient, and the kinetic Reynolds number based on the pulsation frequency. By way of verification, it is shown that for large kinetic Reynolds numbers, the Poiseuille flow may be recovered. Conversely, the purely oscillatory solution by Rott is regained for large pulsation parameters. For sinusoidal pulsations, the flow rate is determined and compared with the steady flow analog obtained under the same pressure gradient. The amount of flow amplification or attenuation is determined as a function of frequency and pulsation parameters. For large frequencies, the maximum flow rate is evaluated and related to the pulsation parameter. By characterizing the velocity, vorticity, and shear stress distributions, cases of flow reversal are identified. Conditions leading to flow reversal are delineated for small and large kinetic Reynolds numbers in both planar and axisymmetric chambers. For an appreciable pulsation rate, we find that the flow reverses when the pulsation parameter is increased to the point of exceeding the Stokes number. By evaluating the skin friction coefficient and its limiting value, design criteria for minimizing viscous losses are realized. The optimal frequency that maximizes the flow rate during pulsing is also determined. Finally, to elucidate the effect of curvature, comparisons between planar and axisymmetric flow results are undertaken. The family of exact solutions presented here can thus be useful in verifying and validating computational models of complex unsteady motions in both propulsive and nonpropulsive applications. They can also be used to guide the design of fuel injectors and controlled experiments aimed at investigating the transitional behavior of periodic flows.

I. Introduction

PULSATORY motions arise in a number of captivating applications involving periodic flow propagation and control [1–10]. Pulsing promotes mixing and therefore mass and heat exchange with the boundaries. Pulsing also reduces surface fouling by facilitating solid particle migration. In the propulsion community, oscillatory flows, which form a subset of pulsatory motions, are routinely used to describe the aeroacoustic field in solid rocket motors [11]. This is especially true of past [12] and recent models [13,14] that have been integrated into combustion stability calculations [15–18]. In other applications, pulse control is used to improve the design of mixers [19], induce particle agglomeration, and facilitate pollutant removal. In recent years, it has been explored in the design of various thermoacoustic devices [20–23].

Clearly, pulsatory flow theory has been the topic of intense research over several decades [24]. In fact, the first mathematical treatment of a simple oscillatory motion may be traced back to Stokes' second problem [25,26]. Both theoretical and experimental studies have, of course, followed, and a summary of their earlier accounts may be found in the surveys by Rott [1] and White [2]. Two particular studies that have been universally cited are those by Womersley [3,4] and Uchida [5]. The former is known for presenting the purely oscillatory solution in a viscous tube, whereas the latter is known for developing a generalized pulsatory solution from which Womersley's formulation may be recovered as a special case.

Received 31 March 2008; accepted for publication 2 June 2008.

*H. H. Arnold Chair of Excellence in Advanced Propulsion, Mechanical, Aerospace, and Biomedical Engineering Department; maji@utsi.edu. Member AIAA.

It should be noted that the 1928–1956 era witnessed the development of several solutions for periodic motions preceding Uchida's [5] work. Accordingly, the first treatment of the oscillatory flow problem of an incompressible fluid in a rigid tube subject to a time-varying pressure gradient may be attributed to Grace [27]. His axisymmetric solution is represented in the form of Kelvin functions. The same oscillatory solution was later obtained independently by Sexl [28], Szymanski [29], and Lambossy [30] in 1930, 1932, and 1952, respectively. Grace [27] was perhaps the first to note that the maximum velocity at any cross section shifts away from the centerline with successive increases in the shear wave number. Experimental verification was provided shortly thereafter by Richardson and Tyler [31]. They reported an annular region near the wall where peak velocities could be observed. The velocity overshoot later came to be known as the Richardson annular effect. The shear wave number has also been referred to as Womersley or Stokes number and its square has been termed frequency parameter, pulsating flow Reynolds number, oscillation, or kinetic Reynolds number. For values of the shear wave number in excess of five, the peak velocity occurred near the wall, thus leading the centerline motion due to the presence of alternating pressure. These studies culminated in Uchida's analysis [5] for arbitrary, time-dependent, axial pressure gradients in pulsatory pipe flows.

In short, Uchida's technique [5] combines the concepts of Fourier decomposition of a complex pressure signal into individual modes and the linearity of the incompressible Navier–Stokes equation for strictly parallel flows. Through linearity, a summation taken over the harmonic frequencies that compose the imposed waveform can thus be used to construct a general solution.

Other theoretical studies by Rao and Devanathan [6] and Hall [7] have used perturbations to develop the pulsatory formulation in a tube with slowly varying cross sections. Also, Ray et al. [32] have considered the inverse problem in which the pulsating mass flow rate is specified in lieu of the pressure gradient. Furthermore, these researchers have conducted well-controlled experiments to confirm the validity of their models. In similar context, Das and Arakeri [33] and Muntges and Majdalani [34] have presented analytical solutions

for the fully developed pulsatory motion driven by a prescribed, time-dependent, volumetric flow rate. Others have incorporated the effects of viscoelasticity [8], wall porosity [9], and wall compliance [10].

It should be noted that, except for Uchida's work in a circular tube [5], other studies have considered the pulsatory motion to be induced by a sinusoidal forcing function of a single-valued frequency. This includes Wang's simplified model of a porous channel wherein the crossflow velocity is taken to be constant throughout the channel [9]. As reaffirmed by Ray et al. [32], no generalization has been carried out in the channel configuration despite its relevance and direct application to practical ducts and laboratory simulations performed in a planar, windowed environment [35,36]. The channel flow analog is clearly useful in modeling slit flows [37], T burners, and combustion chambers with slab propellants [38].

In extending Uchida's work [5], this article will present the exact solution of the two-dimensional Navier–Stokes equations for a channel in which an arbitrary pressure gradient is established. In the process, a comparison with Uchida's generalization will be carried out, so that differences due to curvature effects are illuminated. The analysis will also seek simple closed-form approximations, which are otherwise unavailable in the literature, to describe the principal flow attributes under both axisymmetric and planar configurations. After implementing an original normalization approach that helps to reduce the number of diagrams needed to characterize the problem, closed-form solutions for several salient flow features are derived. These include, for a given set of frequency and pulsation parameters: the flow amplification or attenuation caused by the alternating pressure, the skin friction coefficient, the velocity and vorticity evolutions, the amplitude and phase lag of the shearing stress with respect to the driving pressure gradient, and the conditions leading to flow reversal. These parameters are relevant to several applications ranging from propulsion to biomedical science.

In biologically inspired flows, fluctuating stresses can influence the responsiveness of endothelial cells [39] so profoundly that their accurate determination in a pulsatory environment is considered in a number of investigations concerned with the characterization of atherosclerosis [40–42]. As one cause of this disease is associated with abnormalities in fluctuating stresses [43], identification of the role of flow dynamics is commensurate with pulsatory flow attributes. These are essential to the proper characterization of mechanically assisted respiration [44], hemodialysis in artificial kidneys [9], and peristaltic transport [45]. The same can be said of the purely oscillatory respiratory flow in the larger airways.

In the propulsion community, oscillatory flows are continually used to describe the aeroacoustic field in rocket motors. This is especially true of past [12] and recent models [13] that have been considered in modeling rocket internal ballistics. The interested reader may refer, in that regard, to the works of Chu et al. [46], Apte and Yang [47,48], Majdalani and Roh [17], and Majdalani and Van Moorhem [18]. A characteristic feature of analytical models for oscillatory motions is the linearization of the Navier–Stokes equations before applying perturbative tools to describe the fluctuating field and the relative magnitude of the oscillatory pressure with respect to the mean chamber value (here, the pulsation parameter). In comparison to previous oscillatory flow studies that have relied on linearizations [13,17,18], the parallel flow assumption will enable us to obtain an exact solution that is applicable over a wide range of operating parameters. Specifically, it will no longer be contingent on small amplitude oscillations but rather applicable to an arbitrarily large pulsation parameter.

To proceed, the fundamental equations will be simplified in Sec. II by introducing the assumptions of fluid incompressibility and axial flow. The absence of a transverse velocity component leads to a fully developed profile and the cancellation of nonlinear convective terms. This immediate simplification permits the superposition of temporal features associated with pulsatory motions on the steady and fully developed channel flow. The axial pressure gradient is then expressed, via Fourier series, in terms of sinusoidal functions of time. Normalization and manipulation of the Fourier series follows, leading to a complete representation for the velocity, vorticity, and shearing stresses. In Sec. III, results are presented and occasionally compared with their axisymmetric counterparts. In closing, some comments are given in Sec. IV, along with an outlook toward future research.

II. Formulation

A. Mathematical Model

We consider the incompressible periodic flow in a rectangular channel of height $2a$ and width b. The channel is assumed to be sufficiently long and wide to justify the use of a two-dimensional planar model. We further assume that the pulsatory character is induced by some well-defined pressure gradient caused by "pistons at infinity" [1]. In seeking a laminar solution, we specifically exclude the issue of hydrodynamic instability.

As usual, we take a viscous fluid with density ρ, viscosity $\mu(\nu = \mu/\rho)$, and Cartesian velocity components u and v in the x and y directions. In this study, y will be the normal coordinate measured from the channel's midsection plane. Because the walls are impermeable, the velocity field is everywhere parallel to the x axis. By the same token, the normal velocity v vanishes. The continuity equation becomes

$$\frac{\partial}{\partial x}(\rho u) = 0 \tag{1}$$

Since u cannot vary in the streamwise direction, one must have $u = u(y, t)$ or a fully developed periodic profile. When external forces are ignored, the Navier–Stokes equations reduce to

$$\frac{\partial u}{\partial t} = -\frac{1}{\rho}\frac{\partial p}{\partial x} + \nu\frac{\partial^2 u}{\partial y^2} \tag{2}$$

$$0 = -\frac{1}{\rho}\frac{\partial p}{\partial y} \tag{3}$$

Equation (2) indicates that the pressure gradient must be invariant in x when u is fully developed. Additionally, Eq. (3) renders $p = p(x, t)$. The only form that fulfills Eqs. (2) and (3) is, therefore,

$$\frac{\partial p}{\partial x} = \frac{\partial p}{\partial x}(t) \tag{4}$$

B. Fourier Representation

To accommodate a generally unsteady flow motion caused by some pulsative action, the gradient of the pressure force per unit mass may be equated to an arbitrary function of time; specifically, one may put

$$-\frac{1}{\rho}\frac{\partial p}{\partial x} = p_0 + \sum_{n=1}^{\infty} p_{cn}\cos(\omega n t) + \sum_{n=1}^{\infty} p_{sn}\sin(\omega n t) \tag{5}$$

where p_0 stands for the steady part of the pressure gradient, and p_{cn} and p_{sn} represent the cosine and sine amplitudes of a harmonic forcing function. In the interest of brevity, we put $p_n = p_{cn} - ip_{sn}$ and write

$$-\frac{1}{\rho}\frac{\partial p}{\partial x} = p_0 + \sum_{n=1}^{\infty} p_n \exp(i\omega n t) \tag{6}$$

As usual, the real part of Eq. (6) represents the meaningful solution. Along similar lines, the velocity can be expanded as

$$u = u_0 + \sum_{n=1}^{\infty} u_{cn}\cos(\omega n t) + \sum_{n=1}^{\infty} u_{sn}\sin(\omega n t) \tag{7}$$

where u_0 stands for the steady part of the velocity, and u_{cn} and u_{sn} denote the cosine and sine amplitudes in the corresponding Fourier series. Letting $u_n = u_{cn} - iu_{sn}$, Eq. (7) becomes

$$u = u_0 + \sum_{n=1}^{\infty} u_n \exp(i\omega n t) \tag{8}$$

where the meaningful part is real.

C. Exact Solution

By substituting Eqs. (6) and (8) back into Eq. (2), mean and time-dependent terms may be grouped and segregated. One obtains

$$\sum_{n=1}^{\infty} \exp(i\omega n t)\left(i\omega n u_n - \nu \frac{\mathrm{d}^2 u_n}{\mathrm{d}y^2} - p_n \right) - p_0 - \nu \frac{\mathrm{d}^2 u_0}{\mathrm{d}y^2} = 0 \tag{9}$$

yielding

$$\frac{\mathrm{d}^2 u_0}{\mathrm{d}y^2} + \frac{p_0}{\nu} = 0 \quad \text{and} \quad \frac{\mathrm{d}^2 u_n}{\mathrm{d}y^2} - \frac{i\omega n u_n}{\nu} + \frac{p_n}{\nu} = 0 \tag{10}$$

The preceding set can be readily solved. One finds

$$\begin{cases} u_0 = -\frac{1}{2} p_0 y^2/\nu + C_1 y + C_2 \\ u_n = -\frac{i}{\omega n} p_n + C_{3n} \sinh(y\sqrt{i\omega n/\nu}) + C_{4n} \cosh(y\sqrt{i\omega n/\nu}) \end{cases} \tag{11}$$

In view of linearity, one may combine the elements of Eq. (11) to render

$$u = -\frac{p_0 y^2}{2\nu} + C_1 y + C_2 + \sum_{n=1}^{\infty}\left[-\frac{i p_n}{\omega n} + C_{3n} \sinh\left(y\sqrt{\frac{i\omega n}{\nu}} \right) + C_{4n} \cosh\left(y\sqrt{\frac{i\omega n}{\nu}} \right) \right] e^{i\omega n t} \tag{12}$$

By imposing the appropriate boundary conditions, the remaining constants may be fully determined. For example, at $y = 0$, symmetry demands that $\partial u/\partial y = 0$. It follows that

$$-p_0 y/\nu + C_1 + \sum_{n=1}^{\infty}\left[C_{4n}\sqrt{i\omega n/\nu} \sinh(y\sqrt{i\omega n/\nu}) + C_{3n}\sqrt{i\omega n/\nu} \cosh(y\sqrt{i\omega n/\nu}) \right] e^{iwnt} = 0 \tag{13}$$

hence,

$$C_1 + \sum_{n=1}^{\infty} [C_{3n}\sqrt{i\omega n/\nu}] \exp(i\omega n t) = 0, \quad \forall\ t \quad \text{or} \quad C_1 = C_{3n} = 0 \tag{14}$$

Next, parallel motion must be suppressed at $y = a$ by setting $u = 0$. This implies

$$-\frac{1}{2} a^2 p_0/\nu + C_2 + \sum_{n=1}^{\infty} [C_{4n} \cosh(a\sqrt{i\omega n/\nu} - i p_n/(\omega n)] \exp(i\omega n t) = 0 \tag{15}$$

giving

$$C_2 = \frac{1}{2} a^2 p_0/\nu, \qquad C_{4n} = \frac{i p_n}{\omega n \cosh(a\sqrt{i\omega n/\nu})} \tag{16}$$

At length, one uses backward substitution to deduce the key expression:

$$u(y,t) = \frac{p_0}{2\nu}(a^2 - y^2) + i \sum_{n=1}^{\infty} \frac{p_n}{\omega n} \left[\frac{\cosh(y\sqrt{i\omega n/\nu})}{\cosh(a\sqrt{i\omega n/\nu})} - 1 \right] e^{i\omega n t} \tag{17}$$

Note the distinct differences between Eq. (17) and Uchida's classic solution, reproduced as Eq. (49) in Sec. III.B.

D. Special Case of an Oscillatory Pressure

Given that oscillatory solutions constitute a subset of pulsatory representations, it may be useful to verify that the oscillatory channel flow solution may be restored from Eq. (17). We thus recall the classic theoretical coverage of time-dependent laminar flows by Rott [1] (cf. pp. 401–402). In particular, we consider the oscillatory channel flow that is governed by

$$-\frac{1}{\rho}\frac{\partial p}{\partial x} = K \exp(i\omega n t) \tag{18}$$

In view of Eq. (6), this special case corresponds to

$$p_0 = 0, \qquad p_1 = K, \qquad p_n = 0, \qquad n \geq 2 \tag{19}$$

Direct substitution into Eq. (17) gives

$$u(y,t) = \frac{K e^{i\omega t}}{i\omega}\left[1 - \frac{\cosh(y\sqrt{i\omega n/\nu})}{\cosh(a\sqrt{i\omega n/\nu})} \right] \tag{20}$$

which is identical to Eqs. (3) and (4) in Rott [1]. One may also verify that, for quasi-steady conditions, the fully developed Poiseuille profile may be restored from Eq. (20). This can be realized by extracting the small frequency limit, namely,

$$\lim_{\omega \to 0} \frac{K e^{i\omega t}}{i\omega}\left[1 - \frac{\cosh(y\sqrt{i\omega n/\nu})}{\cosh(a\sqrt{i\omega n/\nu})} \right] = \frac{K}{2\nu}(a^2 - y^2) \tag{21}$$

E. Volumetric Flow Rate

The volumetric flow rate at any cross section can be determined from

$$Q(t) = 2\int_0^a ub\, \mathrm{d}y \tag{22}$$

whence

$$\begin{aligned} Q(t) &= \frac{2p_0 a^3 b}{3\nu} + \frac{2ab}{\omega} i \sum_{n=1}^{\infty} \frac{p_n}{n}\left[\frac{\tanh(a\sqrt{i\omega n/\nu})}{a\sqrt{i\omega n/\nu}} - 1 \right] e^{i\omega n t} \\ &= \frac{2p_0 a^3 b}{3\nu} + \frac{2ab}{\omega} \sum_{n=1}^{\infty} \frac{\sqrt{p_{cn}^2 + p_{sn}^2}}{n} \\ &\quad \times \left[\frac{\tanh(a\sqrt{i\omega n/\nu})}{a\sqrt{i\omega n/\nu}} - 1 \right] e^{i(\omega n t - \theta + \frac{1}{2}\pi)} \end{aligned} \tag{23}$$

where $\theta = \tan^{-1}(p_{sn}/p_{cn})$. Furthermore, for $\omega a^2/\nu > 10$, one may put

$$\begin{aligned} \frac{\tanh(a\sqrt{i\omega n/\nu})}{a\sqrt{i\omega n/\nu}} - 1 &\approx \frac{1}{a\sqrt{i\omega n/\nu}} - 1 \\ &= \frac{1}{\sqrt{ikn}} - 1 = -1 + \frac{1}{\sqrt{2kn}} - \frac{i}{\sqrt{2kn}} \end{aligned} \tag{24}$$

In the foregoing, k is the dimensionless frequency or kinetic Reynolds number [2,49]. It is related to other dimensionless groups via

$$k \equiv \frac{\omega a^2}{\nu} = \alpha^2 = 2\lambda_S^2 \tag{25}$$

where α and λ_S are the Womersley and Stokes numbers, respectively. It should be noted that k is also known as the frequency parameter [1,7–9] or the oscillation Reynolds number [10]. In arterial flows, the Womersley number falls around 3.3 with a corresponding $k \approx 11$ [3,4]. In propulsive applications, k is quite large [50], ranging from 10^4 to 10^8. Consequently, Eq. (23) becomes

$$Q(t) \approx \frac{2a^3b}{3\nu}p_0 + 2\frac{ab}{\omega}\sum_{n=1}^{\infty} Q_n(t) \tag{26}$$

where $\varepsilon = \tan^{-1}(\sqrt{2kn} - 1)^{-1}$ is generally small and

$$\begin{aligned} Q_n(t) &= \frac{\sqrt{p_{cn}^2 + p_{sn}^2}}{n}\left(1 - \frac{2}{\sqrt{2kn}} + \frac{1}{kn}\right)^{\frac{1}{2}} e^{i(\omega nt - \theta - \frac{1}{2}\pi + \varepsilon)} \\ &= \frac{p_n}{n}\left(1 - \frac{2}{\sqrt{2kn}} + \frac{1}{kn}\right)^{\frac{1}{2}} e^{i(\omega nt - \frac{1}{2}\pi + \varepsilon)} \end{aligned} \tag{27}$$

In conformance with the theory of period flows, it can be seen that the flow rate lags the pressure gradient by 90 deg at large frequencies.

To calculate the maximum flow rate in a given cycle, the time corresponding to maximum $Q_n(t)$ may be calculated by setting $\partial Q_n(t_{\max})/\partial t = 0$. For sufficiently large k, one gets

$$\begin{aligned} t_{\max} &= \frac{1}{\omega n}\left[\tan^{-1}\left(\frac{p_{sn}}{p_{cn}}\right) + \frac{\pi}{2} - \tan^{-1}\left(\frac{1}{\sqrt{2kn} - 1}\right)\right] \\ &\approx \frac{1}{\omega n}\left[\tan^{-1}\left(\frac{p_{sn}}{p_{cn}}\right) + \frac{\pi}{2}\right] \end{aligned} \tag{28}$$

Clearly, $t_{\max}$ varies with the mode number n to the extent that each individual contribution Q_n will peak at a different time. Computing the time for which the overall sum $Q(t)$ is largest becomes a root finding problem that may be relegated to a numerical routine. Nonetheless, special cases may be considered for which all Fourier modes $Q_n(t)$ reach their peak at the same time, $t_{\max} = 0$, $\forall\, n$. This condition is characteristic of the family of solutions for which the Fourier coefficients are of the type

$$p_{cn} = 0 \quad \text{and} \quad p_{sn} < 0; \qquad \forall\ n \geq 1 \tag{29}$$

The corresponding $p_{sn}/p_{cn} = -\tan(\pi/2)$, and so $t_{\max} = 0$. The resulting flow rate becomes

$$Q_{\max} = \frac{2p_0a^3b}{3\nu} + \frac{2ab}{\omega}i\sum_{n=1}^{\infty}\frac{p_n}{n}\left[\frac{\tanh(\sqrt{ikn})}{\sqrt{ikn}} - 1\right] \tag{30}$$

and so, approximately,

$$\begin{aligned} Q_{\max} &\approx \frac{2p_0a^3b}{3\nu} \\ &+ \frac{2ab}{\omega}\sum_{n=1}^{\infty}\frac{\sqrt{p_{cn}^2 + p_{sn}^2}}{n}\left(1 - \frac{2}{\sqrt{2kn}} + \frac{1}{kn}\right)^{\frac{1}{2}}; \qquad k > 10 \end{aligned} \tag{31}$$

It may be interesting to note that the mean volumetric flow at a given cross section may be determined by integrating over a cycle, viz.,

$$Q_0 = \frac{\omega}{2\pi}\int_0^{\frac{2\pi}{\omega}} \mathrm{d}t \int_0^a 2ub\,\mathrm{d}y \tag{32}$$

where $2\pi/\omega$ represents a period. Using Eq. (17) and integrating, one gets $Q_0 = \frac{2}{3}p_0a^3b/\nu$. The result coincides with the volumetric flow rate of a steady Poiseuille profile in a channel with a pressure gradient of $\partial p/\partial x = -\rho p_0$. The attendant simplification follows from the cancellation of the oscillatory part while averaging.

F. Normalized Velocity

The time-averaged velocity at any cross section may be calculated from $U = Q_0/(2ab) = \frac{1}{3}a^2p_0/\nu$. This mean value coincides with the average Poiseuille velocity for the same mean flow conditions. Choosing U as a basis for normalization, the nondimensional expression for Eq. (17) becomes

$$u^* \equiv \frac{u}{U} = \frac{3}{2}(1 - \eta^2) + 3i\sum_{n=1}^{\infty}\frac{P_n}{kn}\left[\frac{\cosh(\eta\sqrt{ikn})}{\cosh(\sqrt{ikn})} - 1\right]e^{inT} \tag{33}$$

where

$$\begin{aligned} &\eta \equiv y/a, \qquad T \equiv \omega t, \qquad P_{cn} \equiv p_{cn}/p_0 \\ &P_{sn} \equiv p_{sn}/p_0, \quad \text{and} \quad P_n \equiv P_{cn} - iP_{sn} \end{aligned} \tag{34}$$

At this point, the physical part of Eq. (33) may be extracted and written as

$$\begin{aligned} u^* = \frac{3}{2}(1 - \eta^2) + 3k^{-1}\sum_{n=1}^{\infty} n^{-1}[&A_n(P_{cn}\cos nT + P_{sn}\sin nT) \\ &+ B_n(P_{sn}\cos nT - P_{cn}\sin nT) + P_{cn}\sin nT - P_{sn}\cos nT] \end{aligned} \tag{35}$$

where A_n and B_n are given by

$$\begin{cases} A_n = [\cos(\eta\beta)\sin\beta\cosh(\eta\beta)\sinh\beta - \sin(\eta\beta)\cos\beta\sinh(\eta\beta)\cosh\beta]/D \\ B_n = [\cos(\eta\beta)\cos\beta\cosh(\eta\beta)\cosh\beta + \sin(\eta\beta)\sin\beta\sinh(\eta\beta)\sinh\beta]/D \\ D = \cos^2\beta\cosh^2\beta + \sin^2\beta\sinh^2\beta; \qquad \beta \equiv \sqrt{kn/2} \end{cases} \tag{36}$$

In the limit as $k \to 0$, it can be readily shown (e.g., using symbolic programming) that Eq. (33) reduces to the equivalent Poiseuille form:

$$u^* = \frac{3}{2}\left(1 + \sum_{n=1}^{\infty} P_n\right)(1 - \eta^2) \tag{37}$$

It follows that the exact solution presented here can suitably reproduce both steady and purely oscillatory flow conditions.

G. Relative Volumetric Flow Rate

Equation (37) indicates that, for a steady Poiseuille flow to exhibit the same pressure gradient as that of a pulsatory flow, the mean pressure in the equivalent steady-state problem must be set equal to

$$p_{\text{steady}} = p_0\left(1 + \sum_{n=1}^{\infty} P_n\right) \tag{38}$$

From Eq. (32), one realizes that, for the same pressure gradient, the volumetric flow rate of a steady channel flow will be

$$Q_{\text{steady}} = \frac{2a^3b}{3\nu}p_{\text{steady}} = \frac{2p_0a^3b}{3\nu}\left(1 + \sum_{n=1}^{\infty} P_n\right) \tag{39}$$

Recalling Eq. (30), one can evaluate the ratio of the maximum volumetric flow (due to a periodic pressure gradient) to the corresponding steady flow. Based on Eqs. (29) and (30), one finds

$$Q^* \equiv \frac{Q_{\max}}{Q_{\text{steady}}} = \left[1 + 3i\sum_{n=1}^{\infty}\frac{P_n}{kn}\left(\frac{\tanh\sqrt{ikn}}{\sqrt{ikn}} - 1\right)\right]\left(1 + \sum_{n=1}^{\infty} P_n\right)^{-1} \quad (40)$$

For $k > 10$, this expression is reducible to

$$Q^* \approx \left[1 + 3\sqrt{i}\sum_{n=1}^{\infty}\frac{P_n}{(kn)^{\frac{3}{2}}}\left(1 - \sqrt{ikn}\right)\right]\left(1 + \sum_{n=1}^{\infty} P_n\right)^{-1} \quad (41)$$

or, if its real part is needed,

$$Q^* = 1 + \frac{3}{k}\sum_{n=1}^{\infty}\frac{\sqrt{P_{cn}^2 + P_{sn}^2}}{n}\left[1 - \frac{2}{\sqrt{2kn}} + \frac{1}{kn}\right]^{\frac{1}{2}}\left(1 + \sum_{n=1}^{\infty} P_n\right)^{-1} \quad (42)$$

Equation (41) will be used in the next section to evaluate the asymptotic value of Q^* in the limit as $k \gg 1$.

III. Results and Discussion

For the sake of discussion, two special cases for the pressure forcing function are considered. The first corresponds to a purely sinusoidal (odd) function that satisfies the requirement established by Eq. (29), specifically with $p_{cn} = 0$ and $p_{sn} < 0$, $\forall\, n$:

$$p_{sn} = \frac{p_{sn}}{p_0} = \begin{cases} -\varphi; & n = 1 \\ 0; & n \neq 1 \end{cases} \qquad P_{cn} = \frac{p_{cn}}{p_0} = 0 \qquad \text{(case 1)} \quad (43)$$

The second case corresponds to a mixed pressure gradient involving two harmonic components, namely,

$$P_{sn} = P_{cn} = \begin{cases} \varphi; & n = 1 \\ 0; & n \neq 1 \end{cases} \qquad \text{(case 2)} \quad (44)$$

Here, φ is the pulsation parameter representing the relative importance of the oscillatory pressure gradient with respect to the steady flow contribution. The forms suggested by Eqs. (43) and (44) correspond to sinusoidal pulses that are ubiquitously used in modeling periodic motions [1–5].

A. Flow Attenuation

For case 1, Eq. (40) may be expressed strictly in terms of the frequency and pulsation parameters. After some algebra, one finds

$$Q^* = \frac{1}{k(1+\varphi^2)}\left[k + 3\varphi - \frac{3\varphi}{\sqrt{2k}}\frac{(1+\varphi)\sin(\sqrt{2k}) + (1-\varphi)\sinh(\sqrt{2k})}{\cos(\sqrt{2k}) + \cosh(\sqrt{2k})}\right] \quad (45)$$

The behavior of Q^* is illustrated in Fig. 1 over a range of frequencies and pulsation parameters. This graph confers the general diminution in flow rate modulus (i.e., its maximum value in either direction) with respect to the Poiseuille flow having the same pressure gradient. The reduction in Q^* becomes more important as φ is increased from 0.01 to 100. This is due to the larger contribution of the oscillatory flow component with successive increases in pulse-pressure gradients. Because a self-canceling oscillatory motion does not contribute to a positive volumetric flow rate, increasing the reciprocating part leads to a reduction in Q^*. For $\varphi \leq 0.01$, pulsatory effects become negligible and Q^* approaches the steady-state value of unity. Conversely, for $\varphi \geq 100$, the solution exhibits steeply trailing curves that are characteristic of a nearly oscillatory flow. These observations are in agreement with former studies in channels and pipes that have considered harmonic motions prescribed by single frequencies and pulsation ratios [1–4,6–10]. In our study, the pulsation-dependent curves become closely spaced with successive increases in φ. Because increasing the pulse-pressure gradient φ leads to a predominantly oscillatory solution, it can be argued that increasing the frequency can have a similar impact insofar as it carries the solution further away from its steady-state condition. Consequently, a depreciation in Q^* is generally observed with successive increases in frequency. This diminishment with k becomes more rapid at higher φ when the periodic component of the pressure gradient is intensified. Note that, $\forall\, \varphi$, Q^* levels off asymptotically in k to a fixed "inviscid" limit. In all cases, this inviscid limit $Q^*_{\min}$ may be determined by extracting the expansion of Eq. (41) for an infinitely large k. The result is

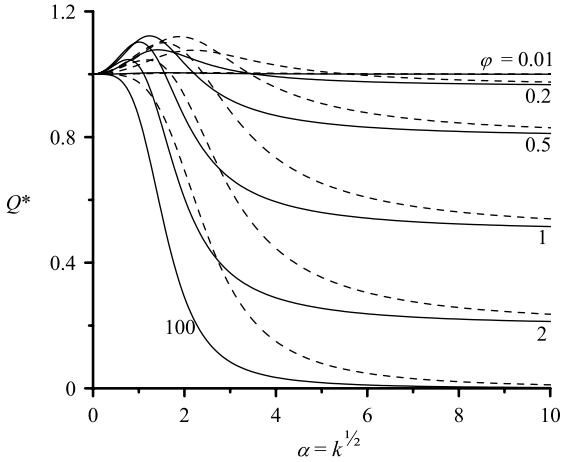

Fig. 1 Effect of varying the frequency and pulsation parameters k and φ on $Q^* = Q_{\max}/Q_{\text{steady}}$; Q^* is the ratio of the maximum flow due to a given pulsatory pressure to the corresponding steady Poiseuille flow for the same pressure gradient. Results are shown for sinusoidal pulsations in both channels (solid lines) and tubes (broken lines).

$$Q^*_{\min} = \left(1 + \sum_{n=1}^{\infty} P_n\right)^{-1} = \frac{1}{1+\varphi^2} \quad (46)$$

The last part of Eq. (46) corresponds to the harmonic motion described by Eq. (43). Thus, for $\varphi = 1$, one obtains a value of $Q^*_{\min} = 0.5$. This prediction matches the value depicted graphically in Fig. 1. On the other side of the spectrum, slow oscillations are manifested by reducing k. Specifically, as $k \to 0$, periodicity becomes virtually absent, to the point of precipitating a quasi-steady solution. However, before the steady-state solution is regained, a slight overshoot in Q^* may be observed so long as $k \leq 2.4743$. This permits the determination of the optimal frequency k^* that is capable of inducing the maximum possible flow at a given pressure pulsation ratio. Using perturbation tools, one obtains, within four significant digit accuracy,

$$k^* = \frac{47,685}{19,274}\varphi\left(\sqrt{1 + \frac{269,836}{270,215}\varphi^{-2}} - 1\right) \quad (47)$$

Conversely, given a prescribed frequency, the optimal pulsation ratio that permits achieving the largest flow may be calculated from

$$\varphi^* = \frac{21}{17k} - \frac{9637}{47,685}k + \frac{87,019}{1.738833525 \times 10^9}k^3 \quad (48)$$

Although each curve in Fig. 1 exhibits its own maximum, the largest value over the entire range of operating parameters occurs at $\varphi^* = 0.577329$ and $k^* = 1.42711$ where $Q^*_{\max} = 1.12353$.

B. Comparison with Uchida's Axisymmetric Solution [5]

Because of the important role of Q^* in characterizing pulsatory flows [1–5,7–9], the analysis previously presented can be repeated

for a circular tube of radius a. Using r to represent the radial coordinate in the axisymmetric flow setting, one can write after Uchida [5],

$$u(r,t)=\frac{p_0}{4\nu}(a^2-r^2)+i\sum_{n=1}^{\infty}\frac{p_n}{\omega n}\left[\frac{I_0(r\sqrt{i\omega n/\nu})}{I_0(a\sqrt{i\omega n/\nu})}-1\right]e^{i\omega nt} \quad (49)$$

where I_0 is the modified Bessel function of the first kind. Dividing by the mean speed $U=a^2p_0/(8\nu)$ one recuperates

$$u^*=2(1-\eta^2)+8i\sum_{n=1}^{\infty}\frac{P_n}{kn}\left[\frac{I_0(\eta\sqrt{ikn}}{I_0(\sqrt{ikn})}-1\right]e^{inT};\qquad \eta\equiv r/a \quad (50)$$

Following Eqs. (38–41), the maximum flow rate for the specified p_n can be calculated from

$$Q^*=\left\{1+8i\sum_{n=1}^{\infty}\frac{P_n}{kn}\left[\frac{2}{\sqrt{ikn}}\frac{I_1(\sqrt{ikn})}{I_0(\sqrt{ikn})}-1\right]\right\}\left(1+\sum_{n=1}^{\infty}P_n\right)^{-1} \quad (51)$$

Then, based on the large-argument expansions [51],

$$\begin{cases} I_0(x)=\frac{1}{\sqrt{2\pi x}}e^x(1+\frac{1}{8}x^{-1}+\frac{9}{32}x^{-2}+\frac{75}{1024}x^{-3}+\cdots) \\ I_1(x)=\frac{1}{\sqrt{2\pi x}}e^x(1-\frac{3}{8}x^{-1}-\frac{15}{32}x^{-2}-\frac{105}{1024}x^{-3}+\cdots) \end{cases} \quad (52)$$

one may use $I_1/I_0\approx 1-(1/2)x^{-1}$ and set, for $k>10$,

$$Q^*\approx\left[1+8\sqrt{i}\sum_{n=1}^{\infty}\frac{P_n}{(kn)^{\frac{3}{2}}}\left(2-\frac{1}{\sqrt{ikn}}-\sqrt{ikn}\right)\right]\left(1+\sum_{n=1}^{\infty}P_n\right)^{-1} \quad (53)$$

Recalling that curvature effects become negligible as $k\to\infty$, it is not surprising that the same inviscid $Q^*_{\min}$ is regained as before in Eq. (46). The difference in this case is that Q^* approaches $Q^*_{\min}$ less rapidly than in the channel. This behavior is reflected in the dashed lines of Fig. 1. For $k\le 5.86$, a slight overshoot in Q^* is observed, as in the planar case. Using similar arguments as before, an optimal frequency k^* can be obtained for which the flow rate is maximized at a given pulsation ratio. One finds

$$k^*=\frac{990}{169}\varphi\left(\sqrt{1+\frac{5408}{5445}\varphi^{-2}}-1\right) \quad (54)$$

The corresponding pulsation parameter that permits achieving the peak value $Q^*_{\max}$ at a given frequency may be similarly determined. One retrieves

$$\varphi^*=\frac{32}{11k}-\frac{169}{1980}k+\frac{33,241}{1.7563392\times 10^9}k^3 \quad (55)$$

In the axisymmetric problem, $Q^*_{\max}=1.12125$ is the largest realizable flow rate induced at $\varphi^*=0.5772$ and $k^*=3.365$. The ability to tune the frequency and pressure pulsation parameters to maximize the flow during pulsing is a clearly desirable characteristic.

C. Velocity Pattern

In the remainder of this study, conditions corresponding to case 2 are used with two nonvanishing harmonic components. This is done in the interest of clarity, owing to the large number of choices that may be suitable for discussion.

The evolution of the velocity given by Eqs. (35) and (44) is illustrated in Figs. 2 and 3 over a range of pulsation and frequency parameters. For each combination of φ and k, the velocity is displayed at 12 equally spaced time lines. In Fig. 2, the pulsation parameter is fixed at $\varphi=1$. This results in an oscillatory flow component that is comparable in size to the steady part, especially at low frequency. In Fig. 2a, $k=1$, and so the oscillatory component is large enough that a negative velocity is realized during a portion of the cycle. When k is increased to 2.6681 in Fig. 2b, pulses are more closely spaced, and the reciprocating velocity component nearly cancels the steady part at one time in the cycle. This precludes the appearance of flow reversal. When k is further increased to 10 in Fig. 2c, both the spatial frequency and amplitude of the oscillatory wave are diminished to the point of producing a quasi-steady profile. As the frequency parameter is further increased to 100 in Fig. 2d, the periodic contribution becomes negligible. This case marks the beginning of the fully developed Poiseuille flow behavior. Hereafter, the flow becomes predominantly steady.

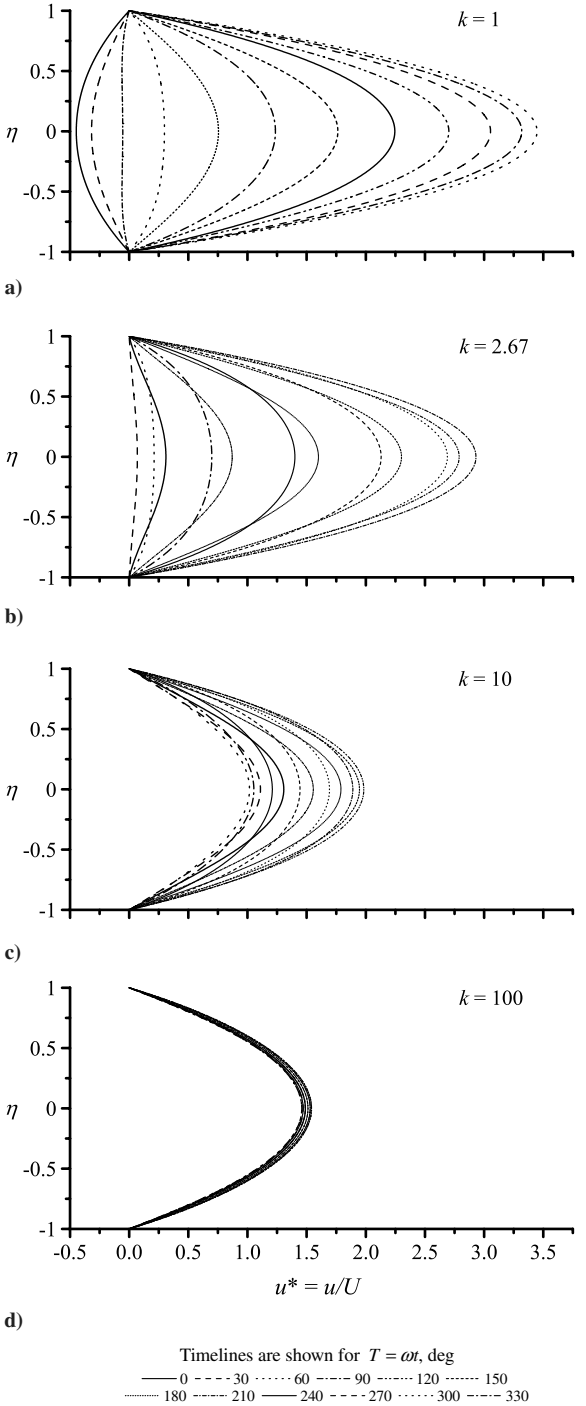

Fig. 2 Nondimensional velocity profiles for $\varphi=1$ and a kinetic Reynolds number of a) 1, b) 2.67, c) 10, and d) 100.

The effect of varying the pulsation parameter at constant k is illustrated in Fig. 3 where φ is reduced from 100 to 0.1. In Fig. 3a, the pulse-pressure gradient is large, relative to its steady counterpart. Under this circumstance, the steady (unidirectional) flow

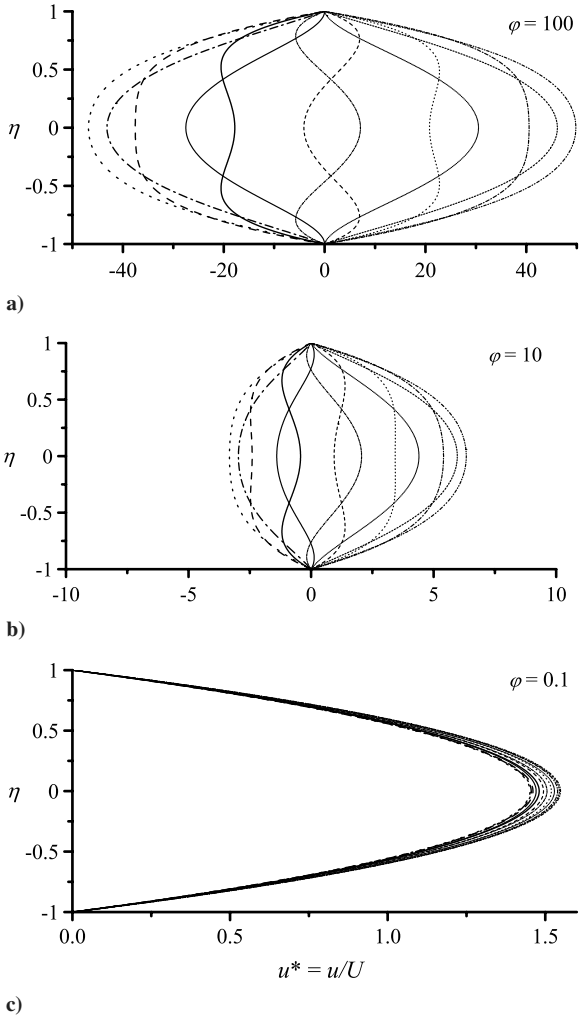

Fig. 3 Nondimensional velocity profiles for $k = 10$ and a pulsation parameter of a) 100, b) 10, and c) 0.1. Time lines are shown using a constant increment of 30 deg as indicated in Fig. 2.

contribution is negligible. The ensuing flow becomes strongly oscillatory, as indicated by the symmetrical time lines in Fig. 3a. The same may be extrapolated for $\varphi > 100$. In fact, for sufficiently large pulsation ratios, the velocity maximum does not occur in the midplane but near the wall, where a mild overshoot may be detected. This overshoot is characteristic of oscillatory flows and has often been named after Richardson [52].

It should be noted that, as the pulsation parameter is reduced to 10 in Fig. 3b, the steady flow contribution is no longer negligible. This is evidenced by the asymmetry in the resulting time lines. As φ is further decreased to 0.1 in Fig. 3c, the pulsation role is reversed. The pulse-pressure gradient is now small in comparison to the steady counterpart. Consequently, a quasi-steady solution is realized. Any further decreases in φ lead to a practically steady flow solution.

D. Vorticity Evolution

From Eq. (33), the vorticity field can be calculated to be

$$\Omega^* = -\frac{\partial u^*}{\partial \eta} = 3\eta + 3\sum_{n=1}^{\infty} \frac{P_n e^{inT}}{\sqrt{ikn}} \frac{\sinh(\eta\sqrt{ikn})}{\cosh\sqrt{ikn}} \tag{56}$$

For the illustrative case specified by Eq. (44), the normalized vorticity time lines are described over a pulsation period in Figs. 4 and 5. Because vorticity is linearly proportional to the shear stress, these plots can be useful in understanding the behavior of the viscous stress as well.

In Fig. 4, the effect of varying the frequency parameter is examined at constant $\varphi = 1$. As shown in Fig. 4a, the vorticity amplitude is large at low frequency. Because of the large oscillatory contribution, vorticity can turn negative, indicating a sign reversal in the direction of rotation. This effect is most pronounced at the surface where it is accompanied, during portions of the cycle, by a reversal in the direction of shear. As the pulsation frequency is increased in Fig. 4b to $k = 2.6681$, the reversal in vorticity is no longer noticeable. Both vorticity and shear become unidirectional. This behavior is more pronounced in Fig. 4c where k is increased to 10; at this frequency, vorticity time lines are more closely spaced. Their spacing and amplitude continue to diminish as k is elevated.

The influence of pulse-pressure gradients on vorticity and shear is examined in Fig. 5 where φ is dropped from 100 to 0.1 at constant k. The large pulse-pressure contribution in Fig. 5a leads to a symmetrical, fully reciprocating vortical character whereby vorticity (and shear) switch direction during half of the cycle. However, when φ is decreased to 10 and below, asymmetry begins to appear because of the growth in the steady pulse contribution. As illustrated in Fig. 5b, unsteady fluctuations in vorticity and shear become miniscule for $\varphi \leq 0.1$. Resulting time-traces gradually collapse closer and closer to the linear distribution connected with a steady, parabolic solution.

E. Skin Friction

By virtue of Eq. (35), the local state of stress exerted by the fluid can be determined from

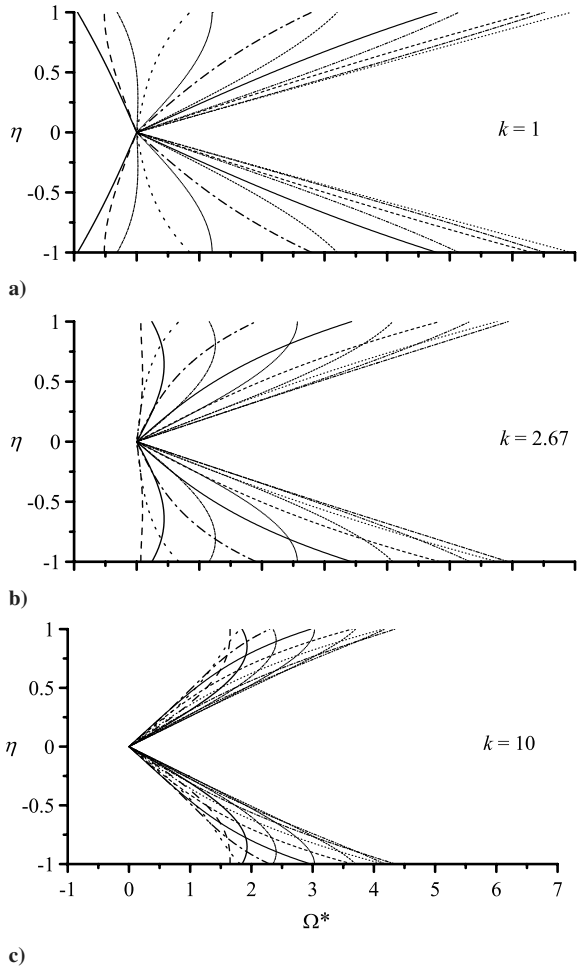

Fig. 4 Nondimensional vorticity profiles for $\varphi = 1$ and a kinetic Reynolds number of a) 1, b) 2.67, and c) 10. Time lines have their usual significance.

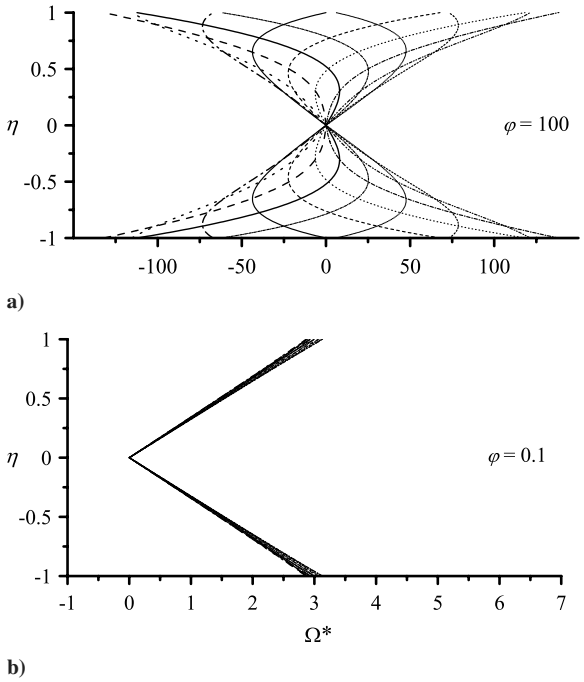

Fig. 5 Vorticity profiles for $k = 10$ and a pulsation parameter φ of a) 100 and b) 0.1. Time lines have their usual significance.

$$\frac{\tau}{\rho U^2} = -\mu\frac{\partial u}{\partial y} = -\frac{\nu}{Ua}\frac{\partial u^*}{\partial \eta} = \frac{2}{Re}\Omega^* = \frac{3\nu^2}{a^3 p_0}\Omega^* \tag{57}$$

where $Re = 2aU/\nu$ is the mean flow Reynolds number. Equation (57) confirms that shear and vorticity are linearly proportional. Instantaneous frictional forces on the wall can be calculated from

$$\frac{\tau_w}{\rho U^2} = \frac{9\nu^2}{a^3 p_0}\left[1 + \sum_{n=1}^{\infty} P_n \frac{\tanh(\sqrt{ikn})}{\sqrt{ikn}} e^{inT}\right] \tag{58}$$

or

$$\tau^* \equiv \frac{\tau_w}{\rho a p_0} = 1 + \sum_{n=1}^{\infty} P_n \frac{\tanh(\sqrt{ikn})}{\sqrt{ikn}} e^{inT} = \frac{1}{3}\Omega^*(a, T) \tag{59}$$

Figure 6 describes the normalized shear stress along the walls of the channel as function of dimensionless time, $T = \omega t$. This is performed over one pulsation period and for a range of k and φ corresponding to the case specified by Eq. (44). It should be noted that the same graph may be used to interpret the vorticity oscillations along the wall since $\Omega^*(a) = 3\tau^*$. In Fig. 6a, increasing the frequency parameter at constant $\varphi = 1$ leads to a faster attenuation of the stress curves. The latter become more closely packed and flatten out eventually at sufficiently high frequencies. The dampening in shear is commensurate with the reduction in velocity and vorticity amplitudes as pulses become more closely spaced. For $k = 1, 2$, the sign reversal in shear indicates a reversal in the direction of motion. However, for $k > 2.6681$ and $\varphi = 1$, a sign reversal is no longer seen. This observation is in agreement with the velocity and vorticity characters described earlier. When φ is varied in Fig. 6b at fixed $k = 10$, a reversal in the sign of shear and, therefore, flow direction, is observed for $\varphi > 2.2234$. As the pulse-pressure gradient is reduced below unity, the shear curves begin to level off. For $\varphi \leq 0.1$, the shear curve is flat, signaling the establishment of steady flow conditions. Similar trends characterize the axisymmetric flow in a tube where the higher surface shear may be calculated from

$$\frac{\tau_w}{\rho U^2} = \frac{32\nu^2}{a^3 p_0}\left\{1 + 2\sum_{n=1}^{\infty}\left[\frac{P_n e^{inT}}{\sqrt{ikn}}\frac{I_1(\sqrt{ikn})}{I_0(\sqrt{ikn})}\right]\right\} \tag{60}$$

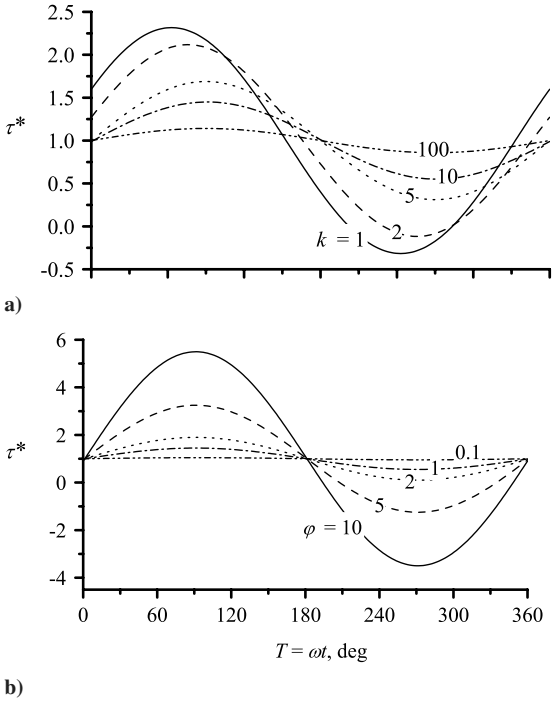

Fig. 6 Effect of varying the frequency and pulsation parameters k and φ on the normalized shear stress at the wall, $\tau^* = \tau/(\rho a p_0)$. This is done at constant a) $\varphi = 1$ and b) $k = 10$.

For the cylindrical configuration, one finds $\Omega^*(a) = 4\tau^*$, indicating that vorticity at the wall is larger than its planar-flow counterpart by one τ^*.

F. Flow Reversal

1. Planar Case

Since τ^* vanishes when the flow switches polarity, the criterion for flow reversal can be determined from Eq. (58). Accordingly, reversal will occur when

$$\mathrm{Re}\left[1 + \sum_{n=1}^{\infty} \exp(inT) P_n \frac{\tanh\sqrt{ikn}}{\sqrt{ikn}}\right] \leq 0 \tag{61}$$

This condition necessitates a sufficiently large pulsation parameter, namely, one that satisfies

$$\varphi \geq \mathrm{Re}[-\tfrac{1}{2}(1+i)\sqrt{ik}\coth\sqrt{ik}\exp(-iT)] \tag{62}$$

In a given cycle, one realizes that the minimum value of φ required to cause flow reversal occurs at

$$T_{\min} = \pi + \tan^{-1}\left(\frac{\sinh\sqrt{2k}}{\sin\sqrt{2k}}\right) \tag{63}$$

This value yields the minimum possible τ_w in a period. Substitution into Eq. (62) provides the reverse-flow criterion,

$$\varphi \geq \mathrm{Re}\{\tfrac{1}{2}(1+i)\sqrt{ik}\coth\sqrt{ik}\exp[-i\tan^{-1}(\sinh\sqrt{2k}/\sin\sqrt{2k})]\} \tag{64}$$

For small and large k, simple approximations can be obtained over the entire range of frequencies. Noting that

$$\tan^{-1}\left(\frac{\sinh\sqrt{2k}}{\sin\sqrt{2k}}\right) \to \begin{cases} \frac{1}{4}\pi + \frac{1}{3}k; & k \to 0 \\ \frac{1}{2}\pi; & k \to \infty \end{cases} \tag{65}$$

one finds

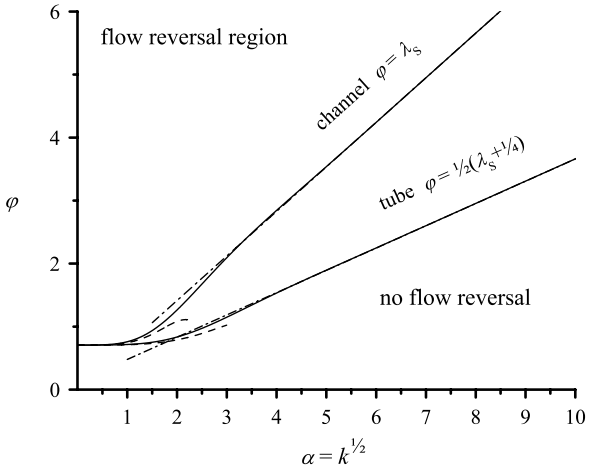

Fig. 7 Identification of flow reversal conditions as function of k and φ. The solid line delineates the region of flow reversal; the broken and chained lines correspond to the small and large asymptotic approximations. Results are for sinusoidal pulsations in both channels and tubes.

$$\varphi \geq \begin{cases} \frac{1}{\sqrt{2}}\left[\cos\left(\frac{1}{3}k\right)+\frac{1}{3}k\sin\left(\frac{1}{3}k\right)\right]; & k \leq 3.74782174 \\ \sqrt{\frac{1}{2}k}=\lambda_S; & k > 3.74782174 \end{cases} \tag{66}$$

These compact expressions entail a maximum error of 12.6% at $k = 3.7478$. Above this value, the flow reverses when the pulsation parameter φ just exceeds the Stokes number λ_S. The relative errors in these approximations drop quickly to 1.9 and 0.55% for $k \leq 1$ and $k \geq 10$, respectively. At $k = 100$, the relative error is just under 7.17×10^{-9}. This makes Eq. (66) practically equivalent to Eq. (64). Both exact and approximate predictions are plotted in Fig. 7 where the region of flow reversal is delineated.

2. Axisymmetric Case

For the tube flow problem, the reverse-flow region may be quantified as well. Based on Eq. (60), one imposes

$$\varphi \geq \mathrm{Re}[-\tfrac{1}{4}(1+i)\sqrt{ik}I_0(\sqrt{ik})\exp(-iT)/I_1(\sqrt{ik})] \tag{67}$$

To make further headway, it is necessary to determine the time for which the right-hand side of Eq. (67) reaches a minimum. One finds

$$T_{\min} = \pi + \tan^{-1}\Theta; \qquad \Theta = \frac{I_0^{\mathrm{Im}}I_1^{\mathrm{Im}} + I_0^{\mathrm{Re}}I_1^{\mathrm{Re}}}{I_0^{\mathrm{Re}}I_1^{\mathrm{Im}} - I_0^{\mathrm{Im}}I_1^{\mathrm{Re}}} \tag{68}$$

where the suppressed argument of the modified Bessel functions is $\sqrt{ik}$; also, superscripts are everywhere used to denote real and imaginary parts. Despite the complexity of Θ, it can be shown, after some algebra, that

$$\Theta = 1 + \frac{1}{4}k + \frac{1}{32}k^2 + \frac{1}{512}k^3 + \cdots \tag{69}$$

Accordingly, reversal will be manifested when

$$\varphi \geq \mathrm{Re}[\tfrac{1}{4}(1-i)\sqrt{ik}I_0(\sqrt{ik})\exp(-i\Theta)/I_1(\sqrt{ik})] \tag{70}$$

This criterion can be replaced by convenient approximations that exhibit a maximum relative error of 4.06% at their upper and lower bounds. Thus, by noting that

$$\tan^{-1}\Theta \to \begin{cases} \frac{1}{4}\pi + \frac{1}{8}k; & k \to 0 \\ \frac{1}{2}\pi; & k \to \infty \end{cases} \tag{71}$$

one extracts

$$\varphi \geq \begin{cases} \frac{1}{\sqrt{2}}\left[\cos\left(\frac{1}{8}k\right)+\frac{1}{8}k\sin\left(\frac{1}{8}k\right)\right]; & k \leq 3.2606845 \\ \sqrt{\frac{1}{8}k}+\frac{1}{8}; & k > 3.2606845 \end{cases} \tag{72}$$

As shown in Fig. 7, it takes less pulse-pressure at the same frequency parameter to induce flow reversal in a tube than in a channel.

G. Friction Coefficient

1. Planar Case

Based on Eqs. (58) and (63), it is possible to determine the maximum skin friction in a cycle. This enables us to use the ratio $C_F = \tau_{\max}/\tau_{\text{steady}}$ to convey the relative importance of surface friction in a pulsatory flow versus a steady flow with the same pressure gradient. For the case at hand, C_F may be determined from

$$C_F = \frac{1 + e^{iT_{\max}}\varphi(1-i)\tanh(\sqrt{ik})/\sqrt{ik}}{1+\varphi(1-i)e^{\frac{1}{4}\pi i}}$$
$$T_{\max} = \tan^{-1}\left(\frac{\sinh\sqrt{2k}}{\sin\sqrt{2k}}\right) \tag{73}$$

The meaningful part of C_F is shown in Fig. 8a at several pulsation and frequency parameters. Near $k \approx 0$, a quasi-steady behavior is expected with $C_F \approx 1$. As the frequency parameter is further increased, C_F decreases due to the trailing role of viscosity. Eventually, an asymptotic limit is reached at sufficiently large frequencies. This lower limit is weakly dependent on the frequency parameter and may be calculated from

$$C_{\mathrm{FL}} = \frac{1+\varphi\sqrt{2/k}}{1+\varphi\sqrt{2}} \tag{74}$$

2. Axisymmetric Case

In the axisymmetric problem, one may follow the same lines by setting

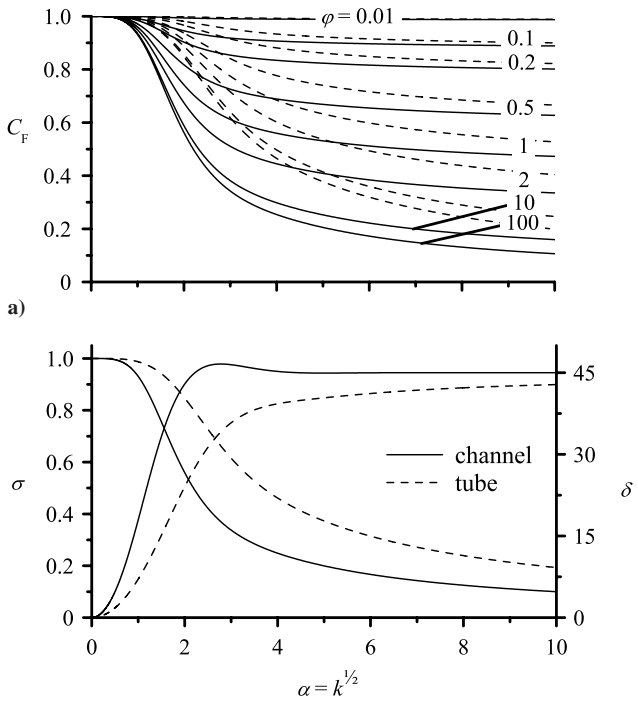

Fig. 8 Effect of varying the frequency and pulsation parameters k and φ on a) the normalized friction coefficient and b) the amplitude and phase of the periodic friction force along the walls. The phase lag is measured with respect to the periodic pressure gradient.

$$C_F = \frac{1 + 2e^{i\tan^{-1}\Theta}\varphi(1-i)I_1/(\sqrt{ik}I_0)}{1 + \varphi(1-i)e^{\frac{1}{4}\pi i}} \tag{75}$$

By analogy with the steady planar-axisymmetric flow differences, it is not surprising that friction due to pulsatory motion in a tube is mildly larger than that in a channel. This is seen in Fig. 8a and can be further confirmed by examining the large frequency limit of the friction coefficient. In fact, from Eqs. (71) and (75), one arrives at

$$C_{\mathrm{FL}} = \frac{1 + \varphi(\sqrt{8/k} - 1/k)}{1 + \varphi\sqrt{2}} \tag{76}$$

which is strictly larger than its planar-flow counterpart. Despite having different initial slopes, it is interesting that both Eqs. (74) and (76) approach the same limit, $(1 + \varphi\sqrt{2})^{-1}$, as $k \to \infty$.

The accurate prediction of the skin friction coefficient and its limiting value can be invaluable in design optimization [49]. By virtue of Eqs. (73–76), one is now able to select an operating frequency that triggers the desired motion, while maintaining an acceptable percentage of the minimum possible amount of energy loss. An optimum frequency may thus be calculated by balancing the cost of producing a given pulsation rate with the cost of overcoming frictional losses.

H. Amplitude and Phase Lag

1. *Planar Case*

Besides the friction coefficient, one may evaluate the often referred to amplitude and phase lag of the shearing stress with respect to the driving pressure gradient [49]. To do so, one rewrites Eq. (59) in phasor form by putting

$$\tau^\star = 1 + P_1 \tanh(\sqrt{ik})e^{iT}/\sqrt{ik} = 1 + P_1\sigma\exp[i(T-\delta)] \tag{77}$$

where

$$\sigma = \frac{\sqrt{\sin^2\sqrt{2k} + \sinh^2\sqrt{2k}}}{(\cos\sqrt{2k} + \cosh\sqrt{2k})\sqrt{k}} \approx \begin{cases} 1 - \frac{7}{90}k^2; & k \le 1.0097321 \\ k^{-\frac{1}{2}}(1 - 4e^{-\sqrt{2k}}\cos\sqrt{2k}); & k > 1.0097321 \end{cases} \tag{78}$$

$$\delta = -\tan^{-1}\left(\frac{\sin\sqrt{2k} - \sinh\sqrt{2k}}{\sin\sqrt{2k} + \sinh\sqrt{2k}}\right) \approx \begin{cases} \frac{1}{3}k - \frac{62}{2835}k^3; & k \le 0.5248009 \\ \frac{1}{4}\pi - 2e^{-\sqrt{2k}}\sin\sqrt{2k}; & k > 0.5248009 \end{cases} \tag{79}$$

Physically, σ and δ represent the amplitude of the wall shearing stress and its phase lag from the pulse-pressure gradient P_1. The asymptotic approximations for small and large k exhibit a maximum relative error of 0.049%. Graphically, they are indiscernible from the exact expressions.

As shown by the solid lines in Fig. 8b, σ decreases at larger kinetic Reynolds numbers. The phase lag, however, increases from 0 to $\frac{1}{4}\pi$ as the frequency is boosted.

2. *Axisymmetric Case*

When the same analysis is repeated for the axisymmetric setting, one obtains

$$\sigma = \frac{2}{\sqrt{k}}\sqrt{\frac{(I_1^{\mathrm{Re}})^2 + (I_1^{\mathrm{Im}})^2}{(I_0^{\mathrm{Re}})^2 + (I_0^{\mathrm{Im}})^2}} \approx \begin{cases} 1 - \frac{5}{384}k^2; & k \le 2.9541846 \\ 2k^{-\frac{1}{2}}[1 - (2k)^{-\frac{1}{2}}]; & k > 2.9541846 \end{cases} \tag{80}$$

where the asymptotic equivalents are derived in an effort to overcome the obscurity of the exact result. These approximations entail an endpoint error of 0.10%. The phase angle can also be evaluated from

$$\delta = -\tan^{-1}\left[\frac{I_0^{\mathrm{Re}}\left(I_1^{\mathrm{Re}} + I_1^{\mathrm{Im}}\right) + I_0^{\mathrm{Im}}\left(I_1^{\mathrm{Re}} + I_1^{\mathrm{Im}}\right)}{I_0^{\mathrm{Im}}\left(I_1^{\mathrm{Re}} - I_1^{\mathrm{Im}}\right) - I_0^{\mathrm{Re}}\left(I_1^{\mathrm{Re}} + I_1^{\mathrm{Im}}\right)}\right] \approx \begin{cases} \frac{1}{8}k - \frac{5}{3072}k^3; & k \le 3.6261113 \\ \frac{1}{4}\pi - (8k)^{-\frac{1}{2}} - \frac{13}{16}k^{-1}; & k > 3.6261113 \end{cases} \tag{81}$$

where the expansions exhibit an endpoint error of 3.9%. As shown in Fig. 8b, both σ and δ approach their large k limits of zero and $\frac{1}{4}\pi$ more gradually than in the channel flow analog. In fact, this behavior may be deduced from Eqs. (80) and (81). In both cases, the phase lag between shear and the pressure gradient is virtually insignificant at low frequencies and approaches 45 deg at high frequencies.

It should be noted that the axisymmetric results developed here reproduce Uchida's pulsatory case [5]. They also agree fairly well with the experimental data for surface friction acquired in the recent study of a fully reciprocating flow in a tube [49]. However, no experimental results could be found to compare with the channel flow solution given here for σ and δ. In this vein, it is hoped that further investigations using controlled experiments of periodic flows could be pursued.

IV. Conclusions

As affirmed by Ray et al. [32], the present article extends the work of Uchida [5] for channel flows by providing results that are otherwise unavailable in the literature. The analysis enables us to quantify several flow attributes at different pulsation parameters. These include salient features that have not been elucidated before. From the expressions entailed for arbitrary pressure gradients in channels and tubes, classic solutions are regained under the limiting conditions that accompany quasi-steady and purely oscillatory behavior. For those solutions that have been previously obtained in an axisymmetric setting, additional features are illuminated. Whenever possible, exact expressions are produced along with nearly equivalent engineering approximations. These include flow attenuation rates, velocities, vorticities, friction coefficients, and phase angles measured with respect to the periodic pressure pulse. Furthermore, the minimum friction coefficient is derived explicitly as a function of the pulsation parameter, and flow reversal is delineated for both axisymmetric and planar flows. In the interest of clarity, comparisons between tube and channel flow properties are brought into perspective. The illustrative case chosen here entails sinusoidal pulsations that are commonly used in practice. In fact, the steps we have undertaken may be repeated in the treatment of more realistic problems in which sophisticated pressure gradients may arise. This is owed to the Fourier analysis, which is fully capable of mapping an arbitrary pressure gradient. Insofar as the final solution is secured in terms of Fourier coefficients, it constitutes a generalization of previous studies based on simple harmonic pulsations.

Aside from its fundamental relevance to the fluid dynamics of periodic flows, the present analysis exposes several characteristic parameters that can be used in a variety of technological applications. These include the development of precise control mechanisms (such as injectors or electronically actuated valves) in studies involving pulse flow velocimetry, laminar-to-turbulent flow transition, fuel injector optimization, mechanically assisted respiration, reverse osmosis, and acoustic wave propagation. Work in this direction is already underway, as some of the parameters described here are being considered in guiding and planning controlled experimental and numerical investigations of pulsatory flow with prescribed pressure or mass flow rates. Examples include those carried out by Ray et al. [32], Ünsal and Durst [53], Ünsal et al. [54,55], and Durst et al. [56].

In the future, it is hoped that the more challenging treatment of a channel with porous walls, variable cross sections, immiscible fluids, and viscoelastic fluids may be separately examined. It is also hoped that experimental data for the pulsatory channel flow will be made available to allow for useful comparisons. Recent work in this

direction by Ray et al. [32] and Durst et al. [57,58] has proven quite instrumental in validating both analytical and numerical solutions of well-controlled periodic flows.

Acknowledgments

This project was sponsored by the National Science Foundation through Grant No. CMMI-0353518 and, through matching funds, by the University of Tennessee Space Institute. The author is deeply grateful for the support received from the National Science Foundation Program Director, Eduardo A. Misawa.

References

[1] Rott, N., "Theory of Time-Dependent Laminar Flows," *High Speed Aerodynamics and Jet Propulsion: Theory of Laminar Flows*, Sec. D, edited by F. K. Moore, Vol. 4, Princeton Univ. Press, Princeton, NJ, 1964, pp. 395–438.

[2] White, F. M., *Viscous Fluid Flow*, McGraw–Hill, New York, 1991.

[3] Womersley, J. R., "Oscillatory Motion of a Viscous Liquid in a Thin-Walled Elastic Tube, I: The Linear Approximation of Long Waves," *Philosophical Magazine*, Series 7, Vol. 46, No. 373, 1955, pp. 199–221.

[4] Womersley, J. R., "Method for the Calculation of Velocity, Rate of Flow and Viscous Drag in Arteries When the Pressure Gradient is Known," *Journal of Physiology*, Vol. 127, No. 3, 1955, pp. 553–563.

[5] Uchida, S., "Pulsating Viscous Flow Superposed on the Steady Laminar Motion of Incompressible Fluid in a Circular Pipe," *Journal of Applied Mathematics and Physics*, Vol. 7, No. 5, 1956, pp. 403–422. doi:10.1007/BF01606327

[6] Rao, A. R., and Devanathan, R., "Pulsatile Flow in Tubes of Varying Cross-Sections," *Journal of Applied Mathematics and Physics*, Vol. 24, No. 14, 1973, pp. 203–213. doi:10.1007/BF01590913

[7] Hall, P., "Unsteady Viscous Flow in a Pipe of Slowly Varying Cross-Section," *Journal of Fluid Mechanics*, Vol. 64, No. 2, 1974, pp. 209–226. doi:10.1017/S0022112074002369

[8] Bhatnagar, R. K., "Fluctuating Flow of a Viscoelastic Fluid in a Porous Channel," *Journal of Applied Mechanics*, Vol. 46, No. 1, 1979, pp. 21–25.

[9] Wang, C. Y., "Pulsatile Flow in a Porous Channel," *Journal of Applied Mechanics*, Vol. 38, No. 2, 1971, pp. 553–555.

[10] Chow, J. C. F., and Soda, K., "Laminar Flow in Tubes with Constriction," *Physics of Fluids*, Vol. 15, No. 10, 1972, pp. 1700–1706. doi:10.1063/1.1693765

[11] Majdalani, J., "Physicality of Core Flow Models in Rocket Motors," *Journal of Propulsion and Power*, Vol. 19, No. 1, 2003, pp. 156–159.

[12] Flandro, G. A., "Effects of Vorticity Transport on Axial Acoustic Waves in a Solid Propellant Rocket Chamber," *Combustion Instabilities Driven by Thermo-Chemical Acoustic Sources*, Vol. NCA 4, HTD 128, American Society of Mechanical Engineers, New York, 1989, pp. 53–61.

[13] Majdalani, J., "Oscillatory Channel Flow with Arbitrary Wall Injection," *Journal of Applied Mathematics and Physics*, Vol. 52, No. 1, 2001, pp. 33–61. doi:10.1007/PL00001539

[14] Majdalani, J., and Flandro, G. A., "Oscillatory Pipe Flow with Arbitrary Wall Injection," *Proceedings of the Royal Society of London A*, Vol. 458, No. 2023, 2002, pp. 1621–1651.

[15] Majdalani, J., Flandro, G. A., and Fischbach, S. R., "Some Rotational Corrections to the Acoustic Energy Equation in Injection-Driven Enclosures," *Physics of Fluids*, Vol. 17, No. 7, 2005, pp. 74102-1-20.

[16] Flandro, G. A., and Majdalani, J., "Aeroacoustic Instability in Rockets," *AIAA Journal*, Vol. 41, No. 3, 2003, pp. 485–497.

[17] Majdalani, J., and Roh, T. S., "Oscillatory Channel Flow with Large Wall Injection," *Proceedings of the Royal Society of London A*, Vol. 456, No. 1999, 2000, pp. 1625–1657.

[18] Majdalani, J., and Van Moorhem, W. K., "Improved Time-Dependent Flowfield Solution for Solid Rocket Motors," *AIAA Journal*, Vol. 36, No. 2, 1998, pp. 241–248.

[19] Franjione, J. G., Leong, C.-W. L., and Ottino, J. M., "Symmetries Within Chaos: A Route to Effective Mixing," *Physics of Fluids*, Vol. 1, No. 11, 1989, pp. 1772–1776. doi:10.1063/1.857504

[20] Yavuzkurt, S., Ha, M. Y., Koopmann, G., and Scaroni, A. W., "Model of the Enhancement of Coal Combustion Using High-Intensity Acoustic Fields," *Transactions of the ASME. Journal of Energy Resources Technology*, Vol. 113, No. 4, 1991, pp. 277–285. doi:10.1115/1.2905912

[21] George, W., and Reethof, G., "On the Fragility of Acoustically Agglomerated Submicron Fly Ash Particles," *Journal of Vibration, Acoustics, Stress, and Reliability in Design*, Vol. 108, No. 3, 1986, pp. 322–328.

[22] Reethof, G., "Acoustic Agglomeration of Power Plant Fly Ash for Environmental and Hot Gas Clean-Up," *Journal of Vibration and Acoustics*, Vol. 110, No. 4, 1988, pp. 552–557.

[23] Tiwary, R., and Reethof, G., "Numerical Simulation of Acoustic Agglomeration and Experimental Verification," *Journal of Vibration and Acoustics*, Vol. 109, No. 2, 1987, pp. 185–191.

[24] Zamir, M., *Physics of Pulsatile Flow*, Springer–Verlag, New York, 2000.

[25] Stokes, G. G., "On the Theory of Oscillatory Waves," *Transactions of the Cambridge Philosophical Society*, Vol. 8, 1847, pp. 441–455.

[26] Stokes, G. G., "On the Effect of the Internal Friction of Fluids on the Motion of Pendulums," *Transactions of the Cambridge Philosophical Society*, Vol. 9, 1851, pp. 20–21.

[27] Grace, S. F., "Oscillatory Motion of a Viscous Liquid in a Long Straight Tube," *Philosophical Magazine*, Series 7, Vol. 5, No. 31, 1928, pp. 933–939.

[28] Sexl, T., "Über Den Von E.G. Richardson Entdeckten 'Annular-effekt'," *Zeitschrift für Physik*, Vol. 61, Nos. 5–61930, pp. 349–362. doi:10.1007/BF01340631

[29] Szymanski, P., "Some Exact Solutions of the Hydrodynamic Equations of a Viscous Fluid in the Case of a Cylindrical Tube (Quelques Solutions Exactes Des Équations De L'hydrodynamique De Fluide Visqueux Dans Le Cas D'un Tube Cylindrique)," *Journal de Mathématiques Pures et Appliquées*, Vol. 11, 1932, pp. 67–107.

[30] Lambossy, P., "Oscillations Forcées D'un Liquide Incompressible Visqueux Dans Un Tube Rigide Et Horizontal. Calcul De La Force De Frottement," *Helvetica Physica Acta*, Vol. 25, No. 4, 1952, pp. 371–386.

[31] Richardson, E. G., and Tyler, E., "Transverse Velocity Gradient near the Mouths of Pipes in Which an Alternating or Continuous Flow of Air is Established," *Proceedings of the Royal Society of London A*, Vol. 42, No. 1, 1929, pp. 1–15. doi:10.1088/0959-5309/42/1/302

[32] Ray, S., Ünsal, B., Durst, F., Ertunc, Ö., and Bayoumi, O. A., "Mass Flow Rate Controlled Fully Developed Laminar Pulsating Pipe Flows," *Journal of Fluids Engineering*, Vol. 127, No. 3, 2005, pp. 405–418. doi:10.1115/1.1906265

[33] Das, D., and Arakeri, J. H., "Unsteady Laminar Duct Flow with a Given Volume Flow Rate Variation," *Journal of Applied Mechanics*, Vol. 67, No. 2, 2000, pp. 274–281. doi:10.1115/1.1304843

[34] Muntges, D. E., and Majdalani, J., "Pulsatory Channel Flow for an Arbitrary Volumetric Flowrate," AIAA Paper 2002-2856, June 2002.

[35] Barron, J., Majdalani, J., and Van Moorhem, W. K., "Novel Investigation of the Oscillatory Field over a Transpiring Surface," *Journal of Sound and Vibration*, Vol. 235, No. 2, 2000, pp. 281–297. doi:10.1006/jsvi.2000.2920

[36] Casalis, G., Avalon, G., and Pineau, J.-P., "Spatial Instability of Planar Channel Flow with Fluid Injection Through Porous Walls," *Physics of Fluids*, Vol. 10, No. 10, 1998, pp. 2558–2568. doi:10.1063/1.869770

[37] Kozinski, A. A., Schmidt, F. P., and Lightfoot, E. N., "Velocity Profiles in a Porous-Walled Duct," *Industrial and Engineering Chemistry Fundamentals*, Vol. 9, No. 3, 1970, pp. 502–505. doi:10.1021/i160035a033

[38] Majdalani, J., and Van Moorhem, W. K., "Laminar Cold-Flow Model for the Internal Gas Dynamics of a Slab Rocket Motor," *Journal of Aerospace Science and Technology*, Vol. 5, No. 3, 2001, pp. 193–207. doi:10.1016/S1270-9638(01)01095-1

[39] Nerem, R. M., and Levesque, M. J., "Hemodynamics and the Arterial Wall," *Vascular Diseases: Current Research and Clinical Applications*, Grune and Stratton, New York, 1987, pp. 295–318.

[40] Dewey, C. F. J., Bussolari, S. R., Gimbrone, M. A. J., and Davis, P. F., "Dynamic Response of Vascular Endothelial Cells to Fluid Shear Stress," *Journal of Biomechanical Engineering*, Vol. 103, No. 3, 1981, pp. 177–185.

[41] Levesque, M. J., and Nerem, R. M., "Elongation and Orientation of Cultured Endothelial Cells in Response to Shear Stress," *Journal of Biomechanical Engineering*, Vol. 107, No. 4, 1985, pp. 341–347.

[42] Levesque, M. J., Sprague, E. A., Schwartz, C. J., and Nerem, R. M., "Influence of Shear Stress on Cultured Vascular Endothelial Cells: The Stress Response of an Anchorage-Dependent Mammalian Cell," *Biotechnical Progress*, Vol. 5, No. 1, 1989, pp. 1–8.

[43] Sprague, E. A., Steinbach, B. L., Nerem, R. M., and Schwartz, C. J., "Influence of a Laminar Steady State Fluid-Imposed Wall Shear Stress on the Binding Internalization, and Degradation of Low Density Lipoproteins by Cultured Arterial Endothelium," *Circulation*, Vol. 76, No. 3, 1987, pp. 648–656.

[44] Drazen, J. M., Kamm, R. D., and Slutsky, A. S., "High Frequency Ventilation," *Physiology Review*, Vol. 64, No. 2, 1984, pp. 505–543.

[45] Fung, Y. C., and Yih, C. S., "Peristaltic Transport," *Journal of Applied Mechanics*, Vol. 35, No. 4, 1968, pp. 669–675.

[46] Chu, W.-W., Yang, V., and Majdalani, J., "Premixed Flame Response to Acoustic Waves in a Porous-Walled Chamber with Surface Mass Injection," *Combustion and Flame*, Vol. 133, No. 3, 2003, pp. 359–370. doi:10.1016/S0010-2180(03)00018-X

[47] Apte, S., and Yang, V., "Unsteady Flow Evolution in a Porous Chamber with Surface Mass Injection, Part 1: Free Oscillation," *AIAA Journal*, Vol. 39, No. 8, 2001, pp. 1577–1586.

[48] Apte, S., and Yang, V., "Unsteady Flow Evolution in a Porous Chamber with Surface Mass Injection, Part 2: Acoustic Excitation," *AIAA Journal*, Vol. 40, No. 2, 2002, pp. 244–253.

[49] Zhao, T. S., and Cheng, P., "Friction Coefficient of a Fully Developed Laminar Reciprocating Flow in a Circular Pipe," *International Journal of Heat and Fluid Flow*, Vol. 17, No. 2, 1996, pp. 167–172. doi:10.1016/0142-727X(96)00001-X

[50] Majdalani, J., "Boundary Layer Structure in Cylindrical Rocket Motors," *AIAA Journal*, Vol. 37, No. 4, 1999, pp. 505–508.

[51] Abramowitz, M., and Stegun, I. A., *Handbook of Mathematical Functions*, National Bureau of Standards, New York, 1964.

[52] Richardson, E. G., "Amplitude of Sound Waves in Resonators," *Proceedings of the Physical Society, London*, Vol. 40, No. 27, 1928, pp. 206–220.

[53] Ünsal, B., and Durst, F., "Pulsating Flows: Experimental Equipment and Its Applications," *JSME International Journal, Series B (Fluids and Thermal Engineering)*, Vol. 49, No. 4, 2006, pp. 980–987. doi:10.1299/jsmeb.49.980

[54] Ünsal, B., Ray, S., Durst, F., and Ertunc, Ö., "Pulsating Laminar Pipe Flows with Sinusoidal Mass Flux Variations," *Fluid Dynamics Research*, Vol. 37, No. 5, 2005, pp. 317–333. doi:10.1016/j.fluiddyn.2005.06.002

[55] Ünsal, B., Trimis, D., and Durst, F., "Instantaneous Mass Flowrate Measurements through Fuel Injection Nozzles," *International Journal of Engine Research*, Vol. 7, No. 5, 2006, pp. 371–380. doi:10.1243/14680874JER00506

[56] Durst, F., Ünsal, B., and Ray, S., "Method for Defined Mass Flow Variations in Time and Its Application to Test a Mass Flow Rate Meter for Pulsating Flows," *Measurement Science and Technology*, Vol. 18, No. 3, 2007, pp. 790–802. doi:10.1088/0957-0233/18/3/031

[57] Durst, F., Ismailov, M., and Trimis, D., "Measurement of Instantaneous Flow Rates in Periodically Operating Injection Systems," *Experiments in Fluids*, Vol. 20, No. 3, 1996, pp. 178–188. doi:10.1007/BF00190273

[58] Durst, F., Heim, U., Ünsal, B., and Kullik, G., "Mass Flow Rate Control System for Time-Dependent Laminar and Turbulent Flow Investigations," *Measurement Science and Technology*, Vol. 14, No. 7, 2003, pp. 893–902. doi:10.1088/0957-0233/14/7/301

J. Oefelein
Associate Editor